Arab J. Nucl. Sci. Appl., Vol. 55, 4, 109-131 (2022)

ISSN 1110-0451

Arab Journal of Nuclear Sciences and Applications

Web site: ajnsa.journals.ekb.eg

(E S N S A)

Geochemical and Spectrometric Characteristics of Natural Radioactivity Levels (^{238}U, ^{232}Th, ^{40}K) of Monzo-Syenogranites from Wadi El-Nabi' Area, Egyptian Nubian Shield

Mohamed Th. S. Heikal[1], A. M. Abu El Ela[1], Aya S. Shereif[1*], Mokhles K. Azer[2] and Ahmed E. Masoud[1]

(1) Geology Department, Faculty of Science, Tanta University, Tanta 31527, Egypt.

(2) Geological Sciences Department, National Research Centre, 12622-Dokki, Cairo, Egypt.

ARTICLE INFO

Article history:

Received: 15th Mar. 2022

Accepted: 14th June 2022

Keywords:

Field measurements; HpGe detector; chemical analysis of ^{238}U, ^{232}Th, ^{40}K, P-D factors; disequilibrium state; recent U-leaching; magmatic and post-magmatic processes Wadi El-Nabi' area; Egyptian Nubian Shield.

ABSTRACT

Wadi El-Nabi' area (˜400km^2) constitutes Precambrian intrusive-extrusive complex related to the Egyptian-Nubian Shield (ENS). It includes ophiolitic serpentinites, felsic-mafic metavolcanics (bimodal metavolcanics), metapyroclastics (metatuffs), metagabbro-diorite complex, olivine gabbros, and troctolites (young gabbros), and monzo-syenogranites (younger granites). The field and lab radiometric measurements of radioelements, and their geochemical characteristics were carried out for (15) samples of monzo-syenogranites (55 km^2) by RS-230 γ-ray spectroscopy, and HpGe detector. Chemical analyses by ICP-MS are also obtained for the studied granitic rocks to verify the concentrations of specific elements and their inter-relationships with (^{238}U (ppm), ^{232}Th (ppm), and ^{40}K (%). Regarding the RS-230 measurements, the of radionuclide concentrations range are (4- 6.6 ppm) for eU, (8.7-14.75 ppm) for eTh, and (3.62- 5.15%) for K%. On the other hand, the chemical analysis for ^{238}U, ^{232}Th (ppm), and ^{40}K%, of monzo-syenogranites give rise to 3.04 ppm for ^{238}U, 9.44 ppm for ^{232}Th, and 1.82 % for ^{40}K%. The field, and lab radiometric measurements, chemical parameters of P, and D-factors (^{226}Ra/^{238}U, and Uc/Ur respectively) give rise to the disequilibrium state is well evident. On the other hand, the chemical interpretations given by multi-variation diagrams among ^{238}U, ^{232}Th, and ^{40}K, as well as selected elements indicate that the origin of the studied radioactive elements are related to the magmatic process, followed by the later post-magmatic process (hydrothermal).

1. INTRODUCTION

Radioactivity is present everywhere since the creation of the earth (billions of years) [1.2]. It is mostly found in felsic plutonic, and volcanic igneous rocks[3,4,5].

Granites contain variable amounts of Ra, Th, and K concentrations, in which many works of literature stress the radioactivity levels in the felsic igneous rocks [3,4,5]. Almost granitic rocks contain accessory minerals such as zircon, monazite, xenotime, allanite, apatite, and K-feldspars that they are bearing radioactive elements[6,7,8].

The purpose of this study is to determine the levels of radioactivity in the studied granite samples collected from different sites of the pluton, in particular along the shear zone. In addition, to deal with (in-depth) the chemical characteristics of the radionuclides; ^{238}U, ^{232}Th, and ^{40}K in Wadi El-Nabi' monzo-syenogranites, as well as to verify the relationship between natural radioactivity levels of U, Th, and K contents, and some specific trace, and rare-earth elements. Finally, to make a comparison among different techniques for radiometric, and chemical data to focus on the genesis of radioactive elements herein.

2. GEOLOGY

Wadi El-Nabi' area (˜400 km^2) (Fig.1) is situated toward the northwestern of Marsa Alam province. This area has attracted many authors [eg.,9,10,11]. They addressed the mineralogy, and geochemistry of almost rock units in this area.

The present area constitutes a Precambrian intrusive-extrusive complex related to Egyptian-Nubian Shield (ENS). It includes ophiolitic serpentinites, felsic-mafic metavolcanics (bimodal metavolcanic), metapyroclastics

Corresponding author: aya.salah@science.tanta.edu.eg

DOI: 10.21608/ajnsa.2022.127687.1561

(metatuffs), metagabbro-diorite complex, olivine gabbros, and troctolites (young gabbros), and monzo-syenogranites (younger granites). Almost rock units exposed are clearly sliced by numerous shear, and/or fault zones trending NW, N-S (in major), and NE (in minor) (Figs. 1, 2a, and b). Firstly, serpentinites occur as exotic blocks within metatuffs as a matrix mélange. Felsic, and Mafic metavolcanics consist of metadacites, metarhyolites, and metabasalts reveal the most common volcanic characteristics, and metamorphism. The metapyroclastics (metatuffs) vary from fine metatuffs to lapilli ones containing crystal, and lithic fragments. Metagabbros, and diorites are massive rocks with green coloration exhibiting hybridization, and deuteric alteration. The olivine gabbros form low-relief hills of whitish green color. Almost exposures are sheared. Finally, monzo-syenogranites (55km^2) occur as elongated stretched outcrops either as fresh massive rocks of low to high relief (up to 650 m.a.s.l) or separated mountainous faulted blocks, mainly extending NW-SE (Fig. 1). It was largely affected by such phases of deformation, and dyke swarms (Fig. 1). They exhibit rich enclaves, and xenoliths of amphibolite, and metavolcanics. This rock unit is highly sheared, and fractured (Figs. 2a, and b). Almost exposures are dissected by quartz veins, aplite, and basaltic dykes trending ENE-WSW, and N-S (in major), and NW (in minor). The contact between the monzo-syenogranites, and its surroundings is intrusive nature enclosing xenoliths, and enclaves from the latter.

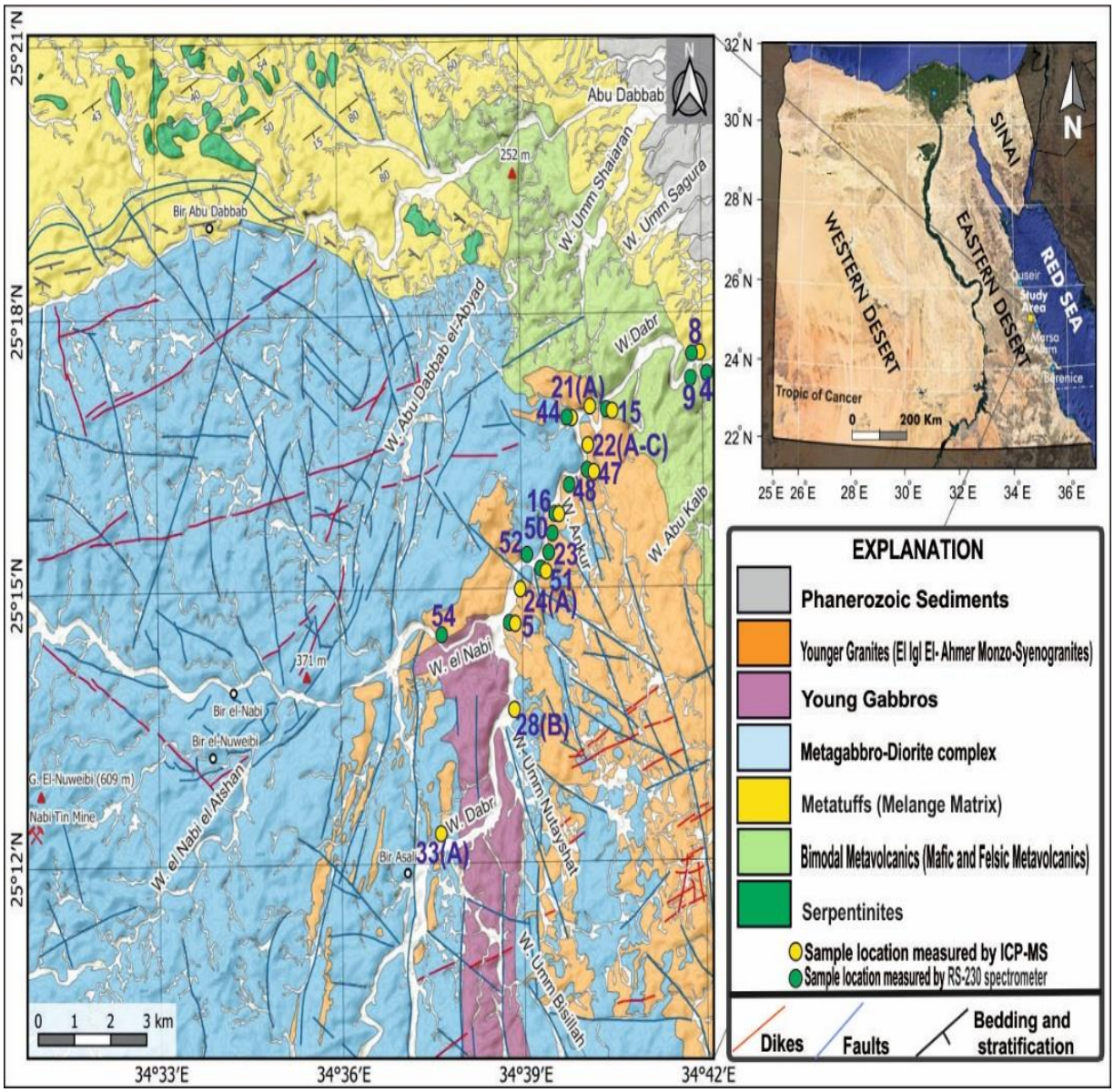

Fig. (1): Location of the point samples measured by RS-230 BGO spectrometer and chemically analyzed by ICP-MS plot on geologic map of Wadi El-Nabi' area.

Fig. (2): (a-b) RS-230 (BGO-SUPER-SPEC) used in the field radiometric measurement of highly sheared monzo-syenogranites.

3. PETROGRAPHIC INSPECTION

3.1. Monzogranite

Microscopically, they are composed of potash feldspar, quartz, and plagioclase together with subordinate meroxene. Sphene, apatite, and zircon are common accessories. **Potash feldspar** (25-30% by volume percent) is mainly of microcline-microperthite forming irregular masses, and plates. **Quartz** (30-40% by volume percent) occurs as anhedral large crystals interstitial to other mineral constituents. Some large quartz crystals split into small individuals, and usually strain shadows, gliding, wavy, and undulose extinction. **Plagioclase** (30-40% by volume percent) is oligoclase (An_{28}) in composition forming tabular crystals. Only slightly altered crystals usually show typical normal zoning (Fig. 3a). Some plagioclase crystals show strain shadows, cracking, and gliding. **Biotite** (meroxene) (<5% by volume percent) occurs either s short flake. It is strongly pleochroic. It is variably altered into, and interleaved with chlorite, and iron oxides along the cleavage. Radioactive halos surrounding zircon enclosed in such crystals (Fig. 3a).

3.2. Syenogranites

Microscopically, these rocks are composed mainly of microcline- microperthite, quartz, plagioclase, and ferro-eddenite together with subordinate astrophyllite (Fig. 3b). Accessories are zircon, apatite, sphene, and iron oxides. **Potash feldspar** (45-50% by volume percent) includes microcline-microperthite of flame type (Fig.3b). It occurs as anhedral plates up to 7 mm across. **Quartz** (25-25% by volume percent) occurs as large anhedral crystals in the form of semicircular embayment, and interstitial spaces up to 9 mm across. Strain shadows giving rise to wavy, and undulose extinction as well as granulation around the borders of other mineral constituents is well remarkable. **Plagioclase** has oligoclase in composition (An_{14}) in the form of tabular crystals up to 8 mm across. Zoning is never elaborate. **Thorite** occurs as shapeless crystals up to 0.5 mm across. It shows faint pleochroism from yellowish brown to dark brown as well as its birefringence is fairly high (Fig. 3c). **Ferro-edenite** is fairly pleochroic. It is highly corroded, and resorbed by quartz, and plagioclase (Fig. 3d).

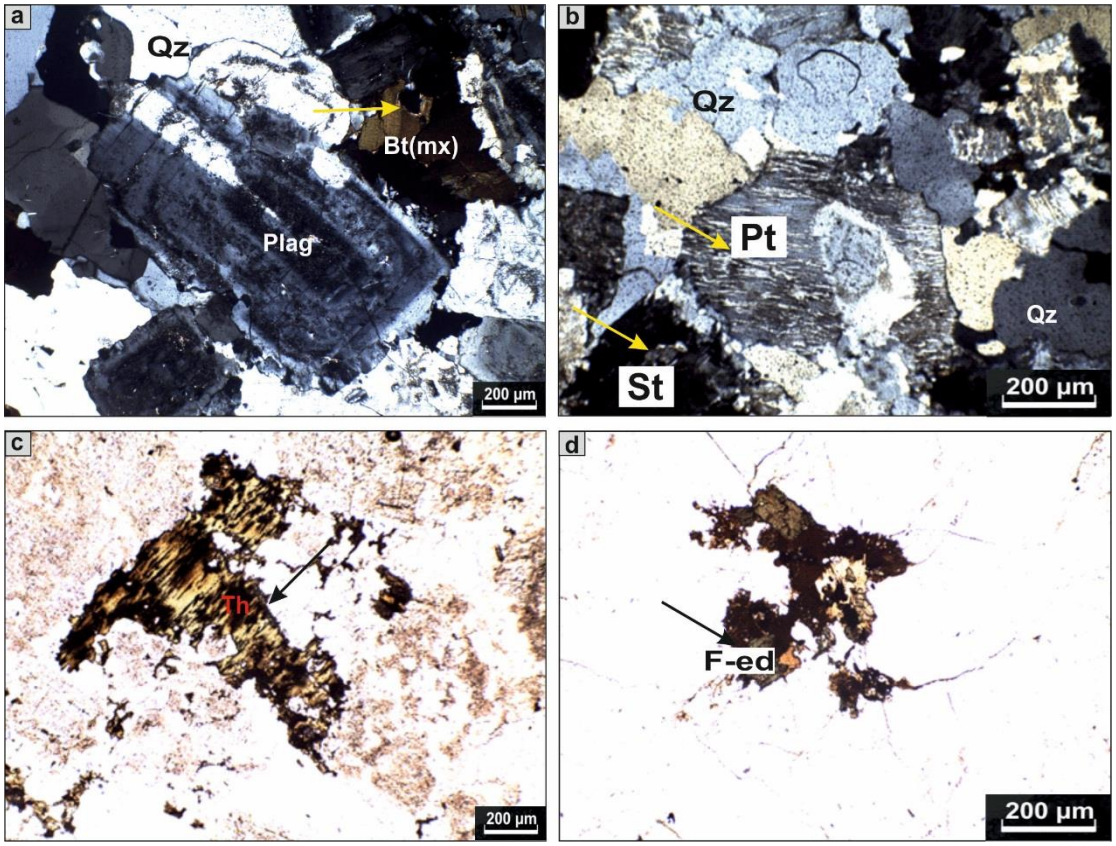

Fig. (3): (a) obvious normal zoning in plagioclase (Plag) in association with quartz (Qz) and meroxene (MX). Monzogranite. XPL, 40x, (b) Typical flame perthitic type (FP) in association with quartz (Qz). Syenogranite. XPL, 40x, (c) Metamict Thorite (Th) in association with Quartz and feldspar indicating volume expansion of Thorite. Syenogranite. PLL, 40x, (d) Ferro-edenite locks like wedge-shaped in association with quartz and feldspar. Syenogranite. PLL, 40x.

4. DIFFERENT ANALYTICAL TECHNIQUES

4.1. Field measurements

Regarding the one of the main approaches of the present work, is a reconnaissance of the radioactivity potential in the studied granitic rocks, using an RS-230 portable detector (Figs. 2a, b, and 4).

The field measurements achieved a radiometric survey of monzo-syenogranites of Wadi El-Nabi', using a portable gamma- ray spectrometer; model RS-230 BGO detector (Bismuth Germanate Oxide) Super-SPEC portable radiation detector and held unit spectrometer survey meter (Figs. 2a, and b) with high accuracy, and its probable measurement, and its errors was about 5%. This detector is full assay capability with data on K%, eU (ppm), and eTh (ppm), with no radioactive sources required for proper operation. The instrument was calibrated using international standards developed by the Geological Survey of Canada (GSC) that are traceable to the IAEA in Vienna. Reference Date for decay correction: 1983-01-30 and Reference Data Sheet: April 1984. These standards ensure consistent, accurate estimates of K, U, and Th [12]. The measurements are based on the detection of γ-radiation emitted in the decay of ^{214}Bi (^{238}U series). Consequently, the deduced amounts of uranium, and thorium are equivalent to what would be in equilibrium with the measured radioactivity of the bismuth or thallium isotopes [13]. Therefore, the term 'equivalent' or its abbreviation 'e' is used to indicate that the equilibrium is assumed between the radioactive daughter isotopes monitored by the spectrometer, and their respective parent isotope.

Regarding the field radiometric measurements of samples (Figs. 2a, and b), and (Table 1), the studied monzo-syenogranites are characterized by radionuclides concentration ranged from 4 to 6.6 ppm with an average of 5.1 ppm for eU, from 8.7 to 15.26 ppm with an average 12.76 ppm for eTh, and from 3.62 to 5.15% with an average 4.43% for K (Table 1, and Fig. 4). We ensured that the higher contents of eU, and eTh are relevant to sheared monzo-syenogranites, whereas massive monzo-syenogranites indicate low values of eU, and eTh (Table 1). The radiometric measurements of the activity measurements have been performed by vertical HpGe detector at Egyptian Atomic Energy Authority (EAEA), Egypt.

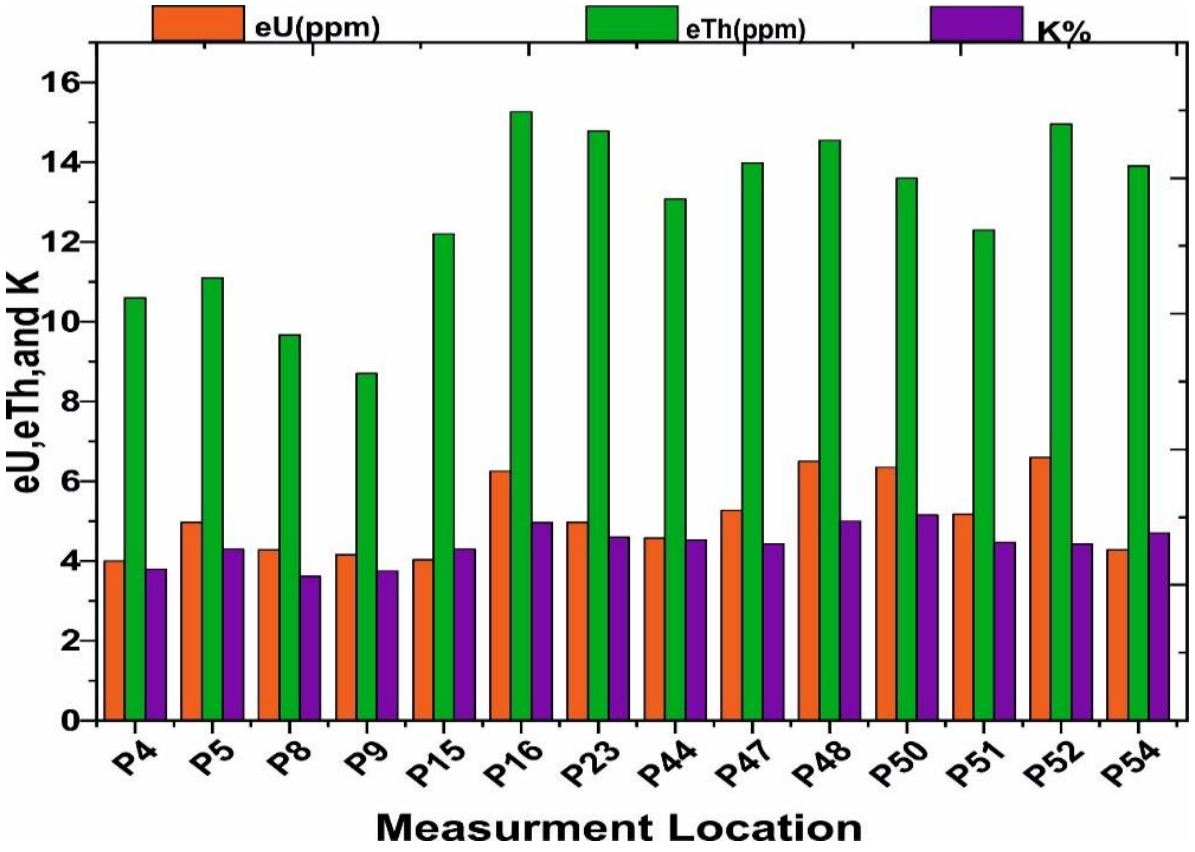

Fig. (4): Histogram for ground spectrometric measurements of eU (ppm), eTh (ppm) and K (%) using RS-230 BGO spectrometer for surface exposure samples of monzo-syenogranites of Wadi El-Nabi'.

Table (1): Average ground gamma-ray spectrometric measurements (K, eU and eTh) for monzo-syenogranites of Wadi El-Nabi' using RS-230 BGO spectrometer.

Points	K%	eU (ppm)	eTh (ppm)	eTh/ eU	eTh/3.5	eTh/K	Latitude-Longitude	Remarks
P4	3.8	4	10.6	2.65	2.03	2.79	25°18′168"N-34°43′400"E	Monzo-Syeno Massive granite cutting with felsic dykes
P5	4.3	4.97	11.1	2.23	3.17	2.58	25°18′103"N-34°43′014"E	Monzo-Syeno Massive granite
P8	3.62	4.28	9.66	2.26	2.76	2.69	25°17′485"N-34°41′948"E	Monzo-Syeno Massive granite
P9	3.75	4.15	8.7	2.09	2.49	2.32	25°17′409"N-34°41′865"E	Monzo-Syeno Massive granite
P15	4.3	4.03	12.2	3.03	3.49	2.84	25°16′965"N-34°40′360"E	Monzo-Syeno Massive granite cutting with mafic dykes
P16	4.96	6.25	15.26	2.44	4.36	3.08	25°15′989"N-34°39′640"E	Monzo-Syeno Sheared Granite cutting with mafic dykes
P23	4.6	4.97	14.78	2.97	4.22	3.21	25°15′630"N-34°39´413"E	Monzo-Syeno Sheared Granite
P44	4.53	4.57	13.08	2.86	3.74	2.88	25°16′952"N-34°40′081"E	Monzo-Syeno Sheared Granite
P47	4.43	5.26	13.98	2.65	3.99	3.15	25˚16′239"N-34°39′987"E	Monzo-Syeno Sheared Granite cutting with dykes
P48	5	6.5	14.55	2.24	4.16	2.91	25°16´212"N-34°39′843"E	Monzo-Syeno Sheared Granite and cavernous granite
P50	5.15	6.35	13.6	2.14	3.89	2.64	25˚16′047"N-34°39′647"E	Monzo-Syeno Sheared Granite
P51	4.46	5.17	12.3	2.38	3.51	2.75	25°15′509"N-34°39′432"E	Monzo-Syeno Sheared Granite
P52	4.42	6.6	14.95	2.27	4.27	3.38	25°15′342"N-34°39′113"E	Monzo-Syeno Sheared Granite cutting with dykes
P54	4.7	4.28	13.9	2.25	3.97	2.96	25°14′418"N-34°37′638"E	Monzo-Syeno Massive granite and gneissose granite
Average	4.43	5.09	12.76	2.53	3.64	2.87	-	-
Mean	4.77	5.39	12.09	2.99	3.95	-	-	-
SD	1.37	1.46	3.26	1.82	0.612	-	-	-

4.2. Geochemistry of Radio-elements

Representative (15) samples of monzo-syenogranites were selected for chemical analysis of some major, trace elements, REEs, and U-Th concentrations at the GeoAnalytical Lab, Washington State University (WSU), USA (Tables 2 and 3). Concentrations of REE and some trace elements were determined via ICP-mass (Agilent7700ICP-MS).

Potash feldspar, zircon, apatite, allanite, sphene, xenotime, and monazite represent the main sources of the light and heavy rare earth elements as well as radioactive concentrations, particularly, ^{40}K, ^{238}U, ^{226}Ra, and ^{232}Th [e.g. 14, 15,16]. Also, the primordial ^{238}U is the most abundant isotope of U (99.27 %) and the initial member of the ^{238}U-decay chain with a long half-life time (4.4683 Ga) [17].

Regarding the chemical analysis of the investigated radioactive and other elements (Table 2), U and Th concentrations in the studied monzo-syenogranites range from 1.86 to 3.04 ppm with an average 2.68 ppm and from 6.25 to 9.44 ppm with an average of 7.76 ppm, respectively (Table 2). In addition, ^{40}K % in the studied rocks vary from 1.29 to 1.82 % with an average 1.44% (Table 2). While the average of Th/U ratios is 2.94 ppm, indicating lower contents, comparing with the average of upper continental crust composition (2.7 ppm for U and 10.5 ppm for Th) [18].

We are going to discuss the given chemical data of ^{238}U, ^{232}Th, and ^{40}K concentrations together with some specific major, trace and rare earth elements in the studied monzo-syenogranites (Tables 2 and 3) for delineating the geochemical characteristics and origin of the radioactive elements herein.

4.2.1. Distribution of radionuclides (^{238}U, ^{226}Ra, ^{232}Th, and ^{40}K)

Radionuclides (^{238}U, ^{226}Ra, ^{232}Th, and ^{40}K) distribution of the studied samples are measured by different techniques; field measurements using portable gamma-ray RS-230 BGO spectrometer, gamma-ray spectroscopy (HPGe detector), and finally chemical analysis using Inductively Coupled Plasma Mass Spectrometry (ICP-MS) (Tables 1-5).

Regarding the field radiometric measurements of samples (Table 1) and the chemical analysis (Table 2) of ^{238}U, ^{232}Th, and ^{40}K of the studied monzo-syenogranites, the calculated values of specific activities of ^{238}U, ^{232}Th, and ^{40}K measured by RS-230 BGO spectrometer and chemical measurements (Fig. 5) indicate that, the radiometric measurement higher than chemical measurement. This attributed to huge background radiation in the studied field area, which arising from primordial radionuclides (uranium, thorium, their decay products, and potassium) as well as cosmic radiation, whereas the measured samples in the laboratory represent a small-size one; about 200 grams for each sample (Table 4 and 5) if compared with large bulk field measured point samples [19,20]. The field radiometric measurements (Table 1) and chemical determination (Table 2), tend to be equal in specific activity and concentrations for massive monzo-syenogranites samples than sheared monzo-syenogranites samples which represent the higher radioactivity concentrations of uranium and thorium if compared with massive monzo-syenogranites samples. This is due to an enrichment that appears to be relevant to the faults, joint, and tension quartz veins [21,22].

With respect of the high concentration of a K% in all studied samples (Table 1), this is due to weathering and alteration processes being inactive leading to almost potash feldspar minerals being still fresh.

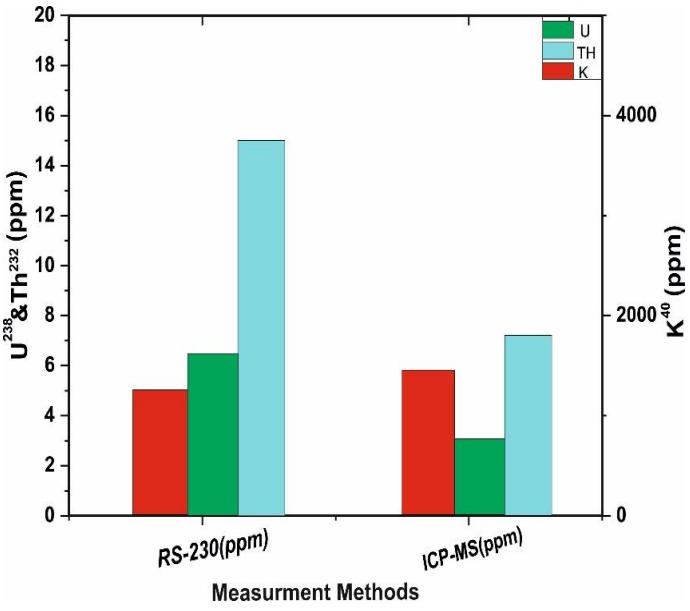

Fig. (5): Average specific activity concentrations (^{238}U, ^{232}Th and ^{40}K) of the studied monzo-syenogranites of Wadi El-Nabi', using radiometric spectroscopy and chemical analysis.

Table (2): Chemical analysis of some major elements, specific activities and their chemical ratios of the studied monzo-syenogranites from Wadi El-Nabi' area, Central Eastern Desert, Egypt.

Sample Number	Sample Type	Na_2O %	K_2O%	A/CNK	K (ppm)	K%	U (ppm)	Th (ppm)	U/Th	Th/U
S8A	Monzogranite	3.46	4.39	1.01	1821.4	1.82	2.79	7.01	0.39	2.51
S15A	Monzogranite	4.08	3.42	1.13	1418.9	1.42	3.04	7.88	0.39	2.59
S16A	Monzogranite	4.11	3.23	1.08	1340.1	1.34	2.54	7.64	0.33	3.01
S22A	Monzogranite	4.19	3.39	1.04	1406.5	1.41	3.03	8.11	0.37	2.68
S22B	Monzogranite	4.18	3.4	1.01	1410.6	1.41	2.61	6.87	0.38	2.63
S22C	Monzogranite	4.22	3.41	1.03	1414.8	1.41	2.88	7.21	0.39	2.50
S24A	Monzogranite	4.21	3.11	0.27	1290.3	1.29	2.54	8.94	0.28	3.52
S28B	Monzogranite	4.16	3.49	1.05	1447.9	1.45	2.78	7.92	0.35	2.85
S44A	Monzogranite	4.21	3.34	1.05	1385.8	1.39	2.81	6.25	0.45	2.22
S44B	Monzogranite	4.23	3.41	1.07	1414.8	1.41	2.99	7.33	0.41	2.45
S51A	Monzogranite	4.26	3.14	1.03	1302.8	1.30	2.79	9.44	0.29	3.38
S16B	Syenogranite	4.24	3.41	1.09	1414.8	1.41	2.34	7.64	0.31	3.26
S21A	Syenogranite	4.24	3.43	1.07	1423.1	1.42	2.43	7.08	0.34	2.91
S33A	Syenogranite	3.51	4.19	1.05	1738.4	1.74	1.86	8.36	0.22	4.49
S47A	Syenogranite	4.01	3.28	1.05	1360.9	1.36	2.84	8.68	0.33	3.06
Average	-	4.09	3.47	1.002	1439.4	1.44	2.68	7.76	0.35	2.94
Mean	-	4.09	3.47	1.002	-	1.44	2.69	7.76	0.35	2.94
SD	-	0.25	0.35	0.21	-	0.15	0.31	0.85	-	0.57

Table (3): Chemical analysis of some trace elements and REEs in monzo-syenogranites of Wadi El-Nabi' area, Central Eastern Desert, Egypt.

Sample	S.T	Rb (ppm)	Nb (ppm)	Ta (ppm)	Y (ppm)	Zr (ppm)	Zr/K%	Zr/U	Zr/Th	Hf (ppm)	LREE (ppm)	HREE (ppm)	ΣREE (ppm)
S8A	Monzogranite	67.2	10.5	0.51	70.7	202.6	111.32	72.62	28.90	8.48	165.31	40.9	206.21
S15A	Monzogranite	75.8	6.5	0.93	38.1	196.3	138.24	64.57	24.91	7.24	109.5	23.84	133.34
S16A	Monzogranite	78.4	7.4	0.68	33.4	176.4	131.64	69.45	23.09	5.9	134.52	23.5	158.02
S22A	Monzogranite	78.4	6.3	0.78	44.1	197.6	140.14	65.21	24.36	6.56	130.86	25.89	156.75
S22B	Monzogranite	76.8	6.8	0.2	39.2	184.6	130.92	70.73	26.87	5.76	115.33	23.62	138.95
S22C	Monzogranite	77.5	7.1	0.61	38.9	192.4	136.45	66.81	26.69	6.15	123.34	25.05	148.39
S24A	Monzogranite	75.8	6.6	0.73	38.1	184.7	143.18	72.72	20.66	5.84	161.24	29.21	190.45
S28B	Monzogranite	80.1	7.2	0.74	40.5	188.9	130.28	67.95	23.85	6.99	114	24.83	138.83
S44A	Monzogranite	72.1	6.9	0.62	37.2	184.7	132.88	65.73	29.55	6.41	123.58	24.31	147.89
S44B	Monzogranite	76.9	6.8	0.77	39.6	185.6	131.63	62.07	25.32	6.24	122.87	24.97	147.84
S51A	Monzogranite	84.2	6.1	0.78	47.1	181.2	139.38	64.95	19.19	5.41	121.59	26.91	148.5
S21A	Syenogranite	79.5	6.6	0.67	36.7	182.7	128.66	75.19	25.81	5.87	112.94	23.1	136.04
S33A	Syenogranite	83.5	5.2	0.45	23.7	64.7	37.18	34.78	7.74	2.71	68.3	14.31	82.61
S47A	Syenogranite	86.4	6.8	0.75	38.4	166.4	122.35	58.59	19.17	5.81	130.73	24.86	155.59
Mean	-	75.91	6.87	0.67	39.95	177.91	-	65.88	23.31	6.15	122.08	25.05	147.13
SD	-	9.49	1.13	0.18	9.97	32.57	-	9.92	5.29	1.23	23.27	5.47	28.21

5. KEY FINDINGS

We are going to delineate the most common radiometric data relationships among specific activities of ^{238}U, ^{232}Th, and ^{40}K (Tables 1 and 2) using variation diagrams for the resultant data obtained by field radiometric measurements.

5.1. Radiometric data

A total (14) points samples for the studied monzo-syenogranites were measured by portable RS-230, giving rise to the concentrations of eU, eTh (ppm), and K % (Table 1). In respect of the localities of point samples (Fig. 1) that are covered almost areal distribution of the studied monzo-syenogranites as well as, they are very close to the locations of samples measured by HpGe detector and also samples subjected to the chemical analysis. Regarding the diagrammatic relationships among these elemental ratios (Figs. 6a-d) for point samples measured are going to follow up:

5.1.1. eU Versus eTh/3.5

(Fig. 6a) reveals a positive correlation indicates U-enriched zones. This is a good agreement by other investigator Abdel-Meguid in 2003 [22].

5.1.2. K (%) Versus eTh

Regarding the Table 1, when eTh/K ≥ 2×10-4, the rock is related to thorium rich, and if eTh/K ≤ 1×10-4, the rock is being potassium-rich [23]. The plots of K (%) versus eTh (Fig. 6b) In the studied monzo-syenogranites is related to thorium-rich rocks.

5.1.3. eU Versus eTh

We found that a positive trend between eTh-eU (Fig. 6c) indicates magmatic process play the main role in radioelements distribution. On the other hand, the average value of eTh/eU ratio for the studied granitic rocks is 2.53, confirming relatively uranium enriched rocks (Table 1).

5.1.4. eTh/eU Versus eTh

The plots of eTh/eU versus eTh diagram exhibit a positive correlation (Fig. 6d) confirming the magmatic process for the studied monzo-syenogranites. This is in the good agreement mentioned by [24].

On the other hand, the average of eTh/eU ratio of all samples (Table 1) is less than Clark's value of 3,5 which indicate enrichment of uranium of the studied granitic samples [21,22].

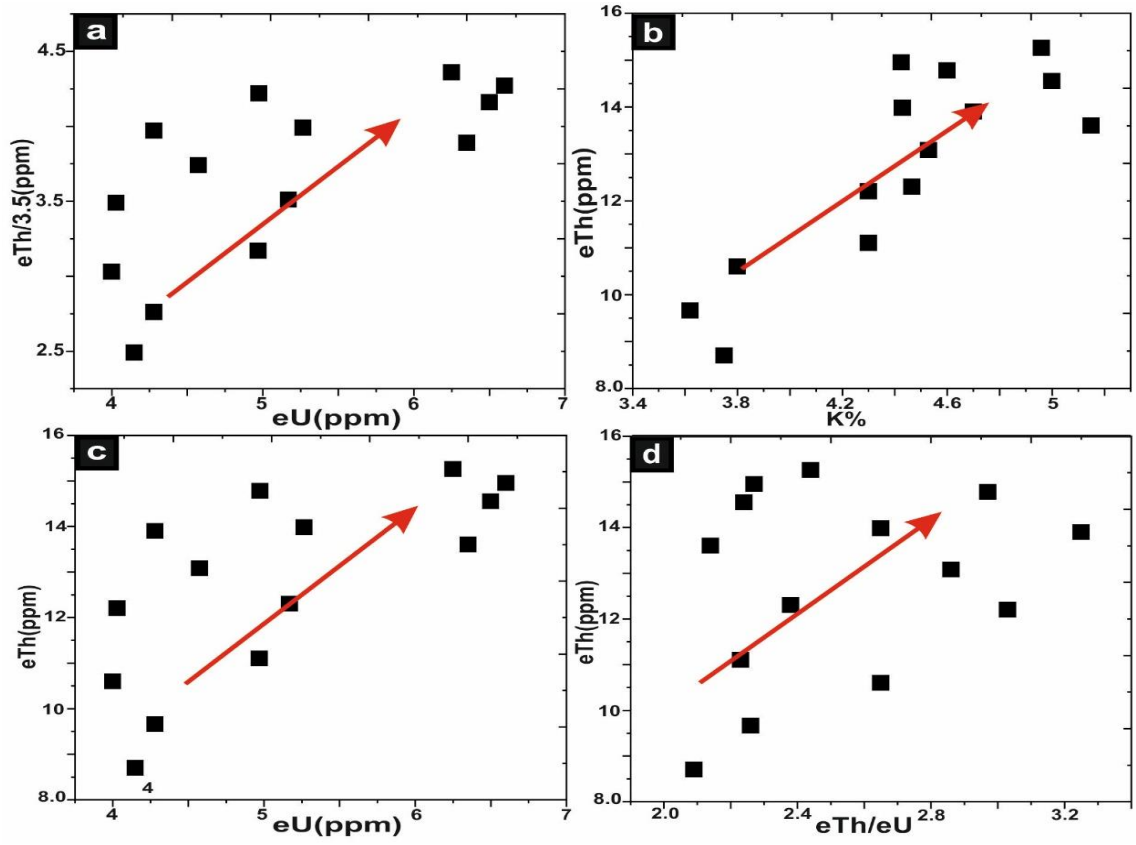

Fig. (6a-d): Variation diagrams of eU, eTh (ppm) and K% relevant to portable γ-ray RS-230 BGO spectrometer for point samples of monzo-syenogranites of Wadi El-Nabi'.

5.2. Chemical interpretations

5.2.1. ^{238}U versus ^{232}Th

Regarding the given chemical data of U, Th, and K concentrations (ppm) for the studied monzo-syenogranites (Table 2) and (Figs. 7a and b), it is evident that the increasing trend of U concentrations meets the increasing trend of Th (Fig. 7a) this reflects magmatic process [24]. On the other hand, the relation U versus (U-Th/3.5) (Fig. 7b) reveals uranium enrichment for the studied monzo-syenogranites.

5.2.2. Alumina saturation index in relation with ^{238}U, ^{232}Th, and ^{40}K

The plots of molecular ratios of Al_2O_3/ (CaO + Na_2O + K_2O) symbolic as A/CNK versus ^{238}U, ^{232}Th and ^{40}K (Fig. 8a, b, and c) and Table (2) indicate a slight positive correlation between A/CNK with ^{238}U and ^{40}K, this suggested that the studied samples with higher A/CNK values have the highest concentrations of ^{238}U and ^{40}K (Figs. 8a and c). Whereas the slight negative correlation is apparently obvious between A/CNK and ^{232}Th (Fig.8b), the higher A/CNK values have the lowest concentrations of ^{232}Th. This is a good agreement by [3, 25].

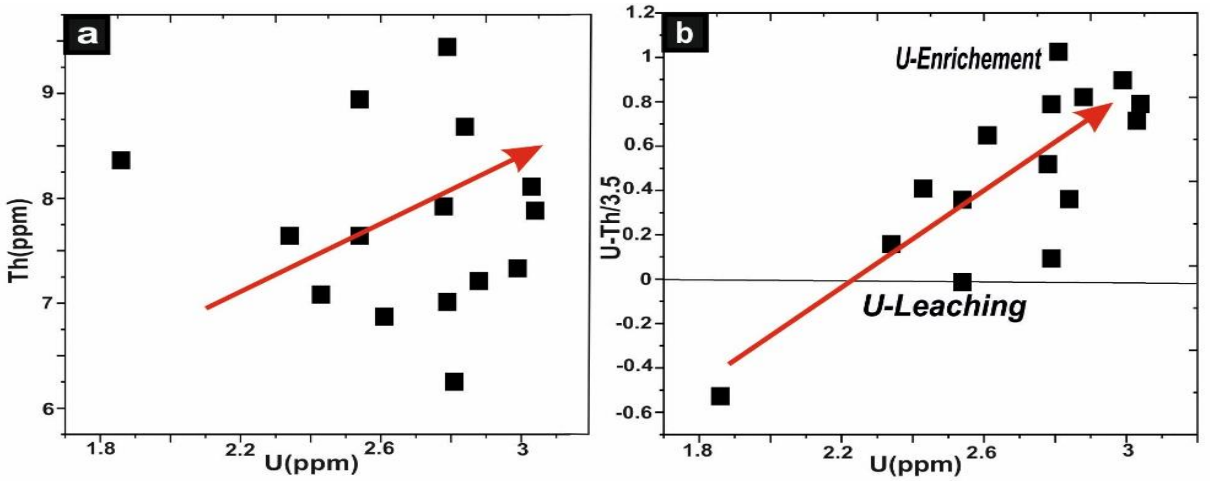

Fig. (7): (a) Variation diagrams between U, Th (ppm) relevant to chemical analysis using ICP-MS technique for monzo-syenogranites, (b) Variation diagrams between U, U-Th/3.5 (ppm) relevant to chemical analysis using ICP-MS technique for monzo-syenogranites. Line separating between U-enrichment and U-leaching in Fig. 7b), after Boyle, 1982.

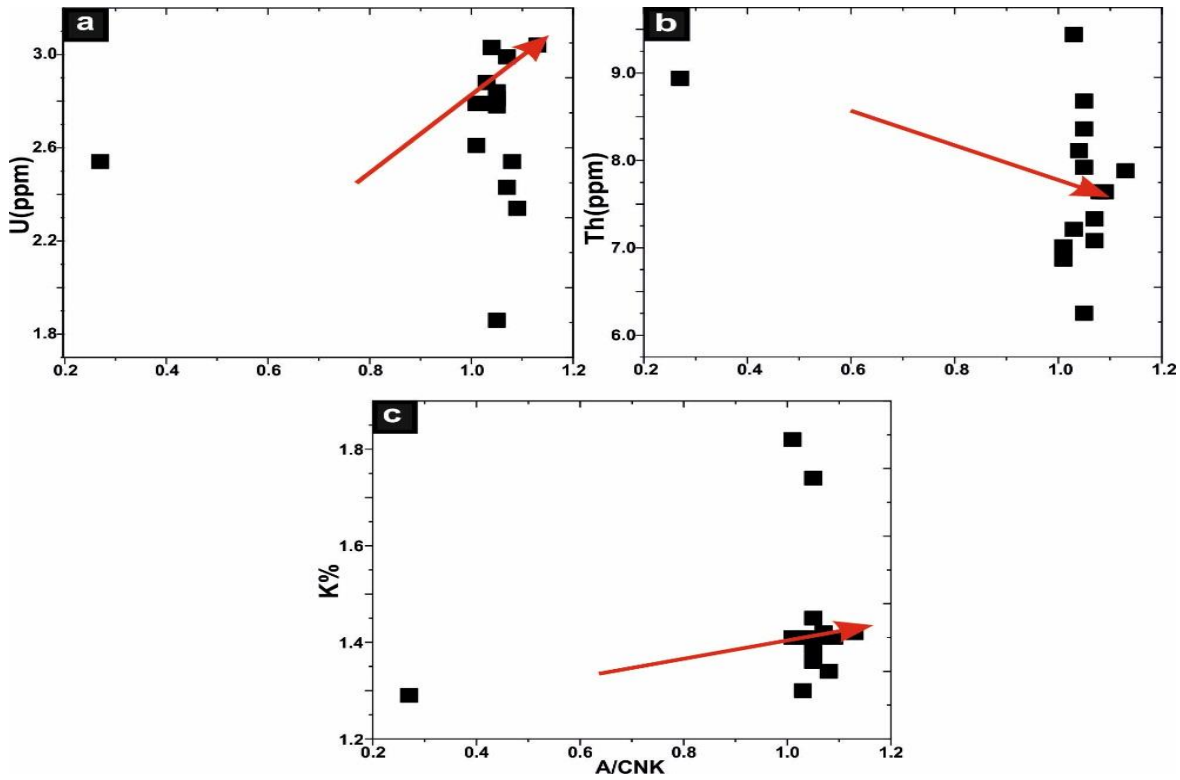

Fig. (8): (a) A/CNK vs. U (ppm), (b) A/CNK vs. Th (ppm) and (c) A/CNK vs. K% of the studied monzo-syenogranites of Wadi El-Nabi'. A/CNK = molar ratio of Al_2O_3/ (CaO + Na_2O + K_2O)

5.2.3. Correlations between radionuclides, and chemical elements

The present radionuclides (^{238}U, ^{232}Th, and ^{40}K) have been correlated with some chemical elements (Tables 2, and 3), and (Figs. 9 to 15).

The studied granitic rocks are characterized by high contents of Na_2O ranging from 3.46 to 4.26 wt. %, low to moderate contents of K_2O varying from 3.11 to 4.39 wt.% up to (4.39 wt.%), whereas CaO and Fe_2O_3 have low contents (Table 2).

With respect of the Na_2O % versus U (ppm) and Th (ppm) (Figs. 9a and b), the positive correlation is well obvious for both, whereas a mild negative correlation between K_2O % and U (ppm) and Th (ppm) (Figs. 9c and d).

Th/U versus Th and U (ppm) (Figs. 10a and b) indicates a positive trend (Fig. 10a) and a negative trend (Fig. 10b). On the other hand, we found positive trends for U-Th and SiO_2-Zr diagrams (Figs. 10c and d). These correlations indicate that the studied granitic rocks have relatively high variation in Th (ppm) content while the U (ppm) content of these rocks appears to be poorly variable.

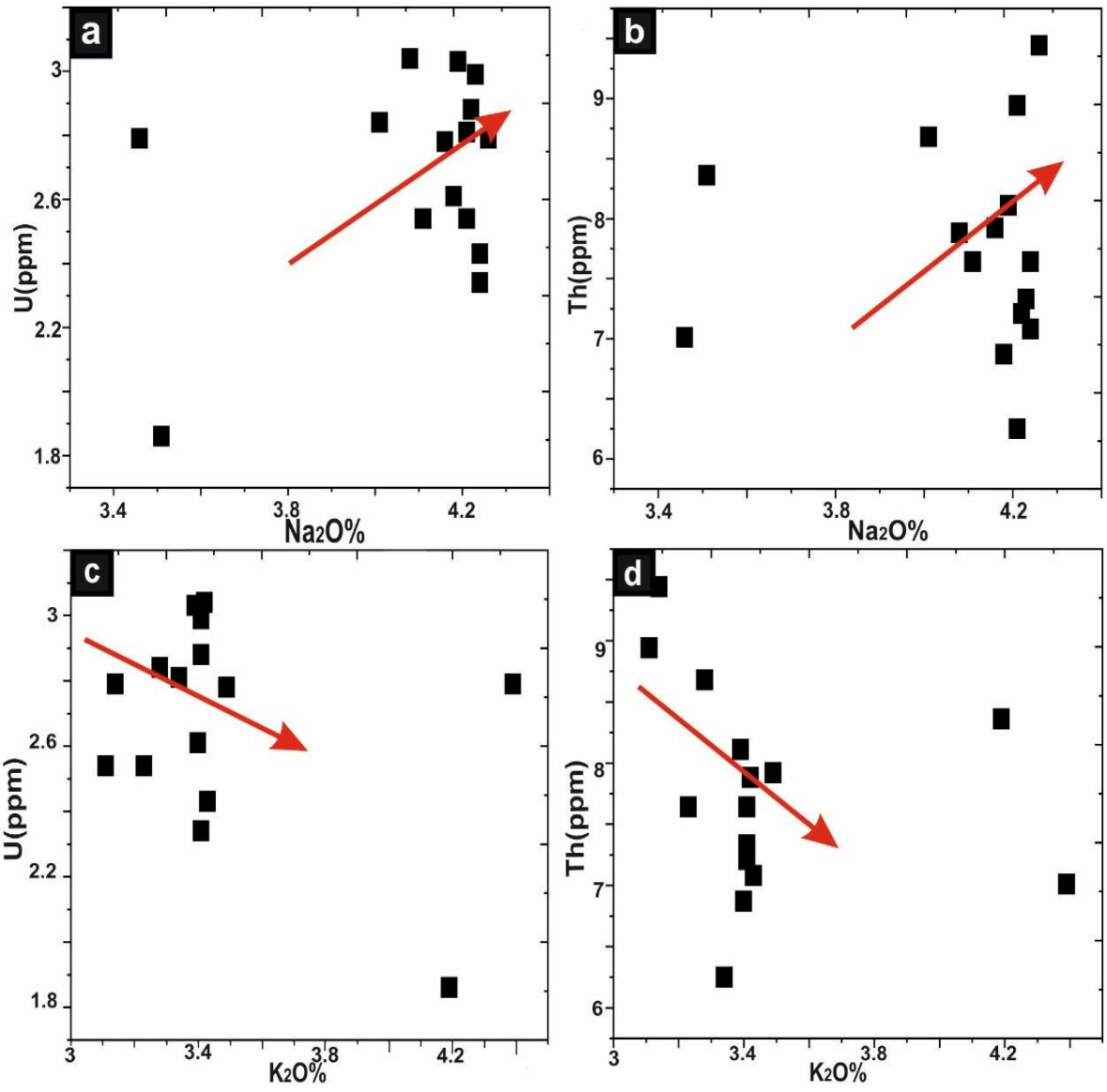

Fig. (9a-d): Variation diagrams among U and Th (ppm) and some major oxides (wt.%) of the studied monzo-syenogranites of Wadi El-Nabi'.

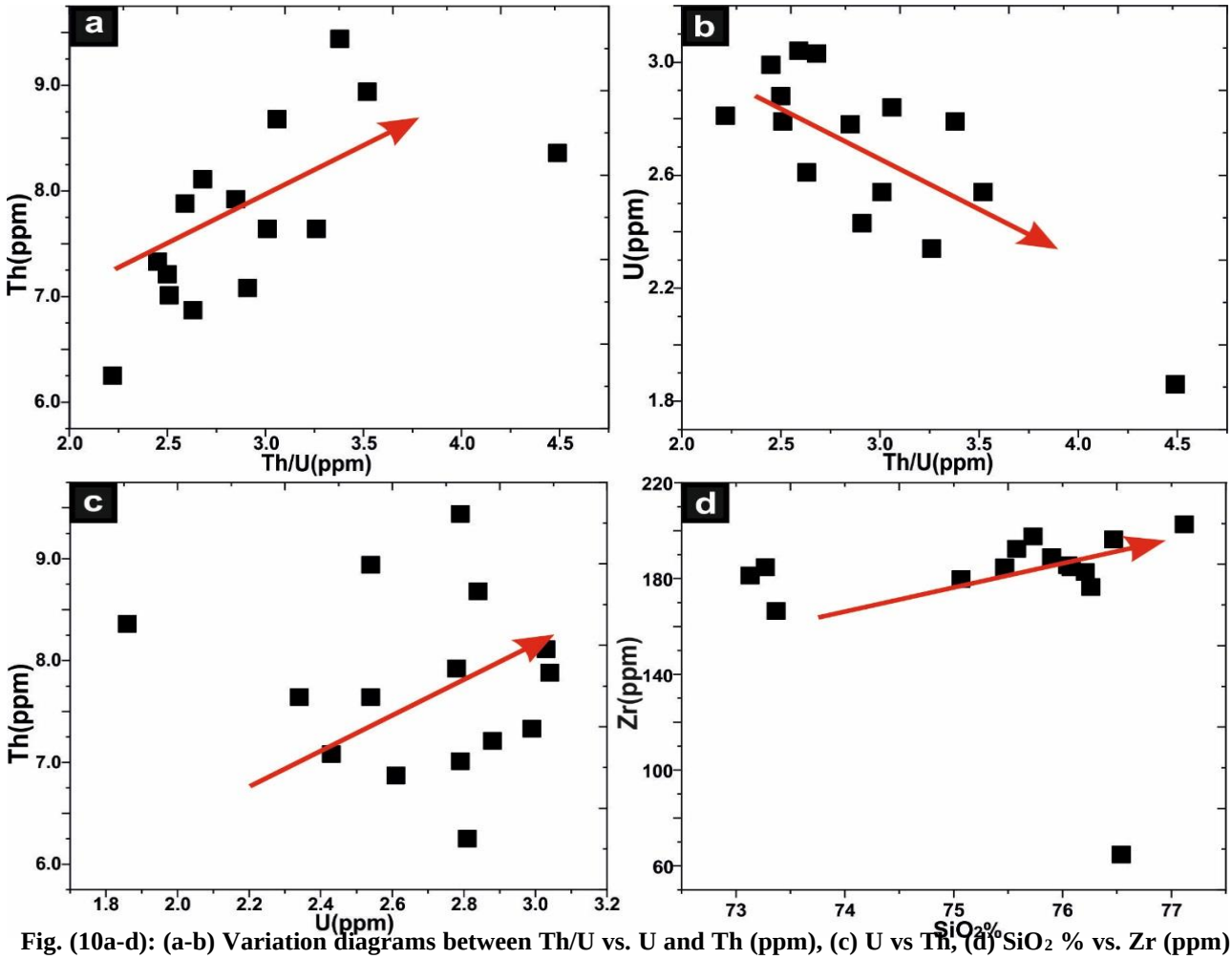

Fig. (10a-d): (a-b) Variation diagrams between Th/U vs. U and Th (ppm), (c) U vs Th, (d) SiO_2 % vs. Zr (ppm) for monzo-syenogranites of Wadi El-Nabi'.

In respect of some trace elements; Nb, Ta, Zr, Hf, Rb and Y and REES (LREEs), (HREEs) and (ΣREEs) versus ^{238}U, ^{232}Th and ^{40}K (Figs. 11 to 15), the studied granitic rocks are characterized by variable contents of Rb, Ta, Nb and Zr (up to 86.4 ppm, 0.93 ppm, 10.5 ppm, and 202.6 ppm) respectively, (Table 3). Whereas ΣREEs have lower values (up to 206.21 ppm) (Table 3).

Regarding the variation diagrams between U and some trace elements (Nb, Ta, Zr, Zr/U, Y, Hf, and Rb ppm) (Figs. 11a-g) reveal a positive correlation with Nb, Ta, and Rb (Figs. 11 a, b and g) and mild positive relation with Zr, Y and Hf (Fig. 11c, e and f), indicating magmatic processes (Zr and Hf) followed by post magmatic processes. On the other hand, there is a decreasing trend between U (ppm) and Zr/U (Fig. 11d).

With respect of Th (ppm) versus the same trace elements mentioned above (Figs. 12a-g); the plots reveal a positive correlation with Ta, Y, Hf, and Rb (Figs. 12b, e, f and g) and negative relation with Nb, Zr, and Zr/Th (Figs. 12a, c and d).

Variation diagrams between K% and the same trace elements mentioned above (Figs. 13a-g) reveal a positive correlation (Figs. 13a-g).

The variation diagrams between Th/U and some trace and rare earth elements (Figs. 14a-i) reveal a negative correlation with some trace elements such as (Nb, Zr, Y and Hf ppm) (Figs. 14a, c, d, and f) and a positive correlation with the other trace elements and REEs (Figs. 14b, e, g, h and i).

The variation diagrams among U and Th (ppm) versus light rare earth elements, heavy rare earth elements, and their total (Figs. 15a-f) reveal a strong positive relation with U (ppm) (Figs. 15a, c and e), and show also a mild positive correlation with Th (ppm) (Figs. 15b, d and f).

5.2.4. Correlations of Radio-elements [^{40}K, and ^{226}Ra (Bq/Kg)] with some chemical elements.

Based on the data of the radiometric measurements using HPGe detector to [^{40}K and ^{226}Ra (Bq/Kg)] (Tables 4 and 5). Firstly, ^{40}K (Bq/Kg) versus some

trace elements (ppm) and major oxides (wt.%) (Figs. 16 a-f), K-40 contents within the studied monzo-syenogranites increase with increasing K_2O %, CaO %, SiO_2 %, and Rb (ppm) (Figs. 16a, c, d and e) while with Na_2O % and Ba display a strong depletion (Figs. 16b and f). This means that no albitization does occur. High potassium contents with increasing ^{40}K values are due to enrichment of k-feldspar. Secondly, the Y, Zr (ppm), and SiO_2 % versus ^{226}Ra (Bq/Kg) diagrams (Figs. 17a-c), displays a positive trend with increasing ^{226}Ra. This is attributed to the magmatic process [e.g., 3,5].

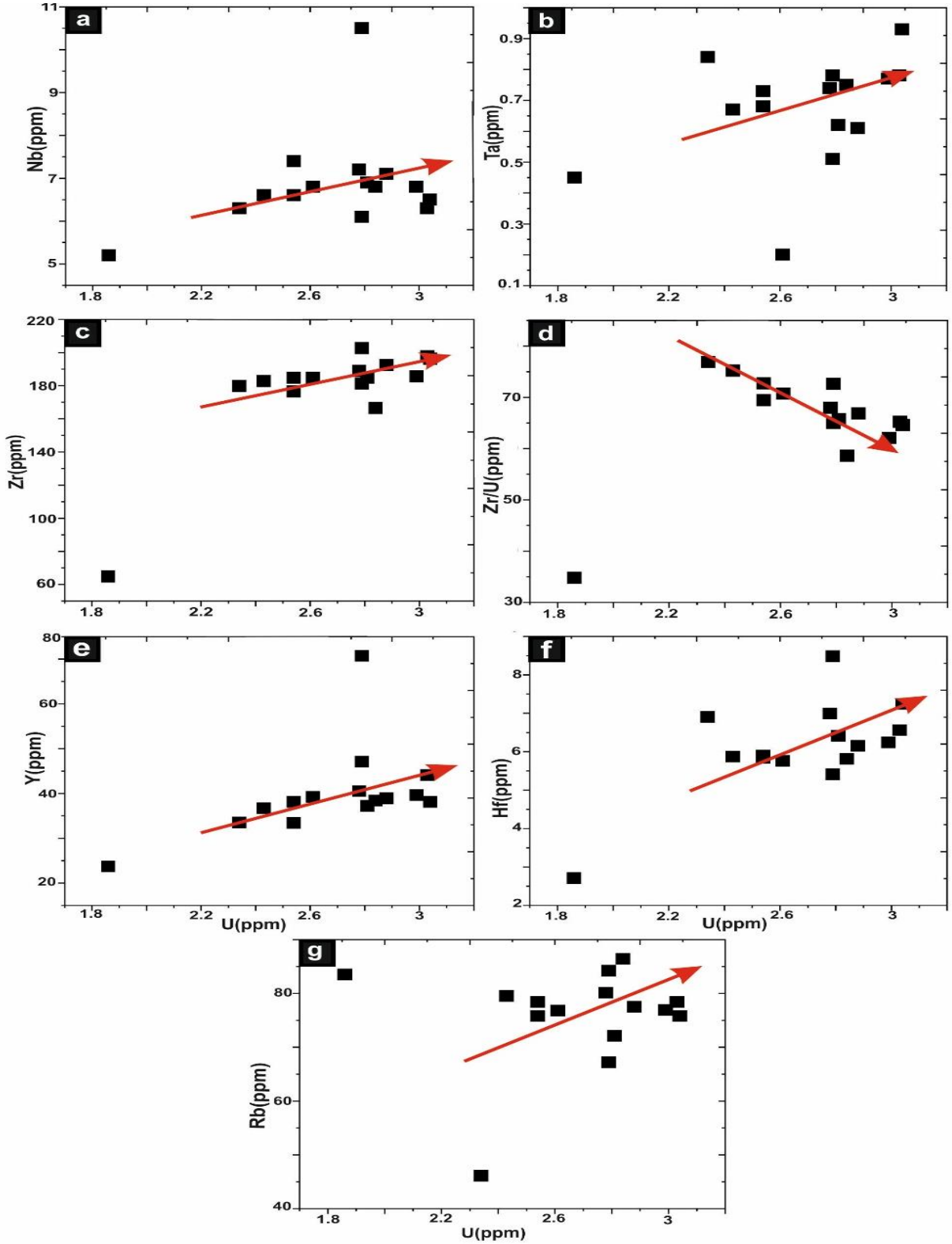

Fig. (11a-g): Variation diagrams between U (ppm) vs. some trace elements (ppm) of monzo-syenogranites of Wadi El-Nabi'.

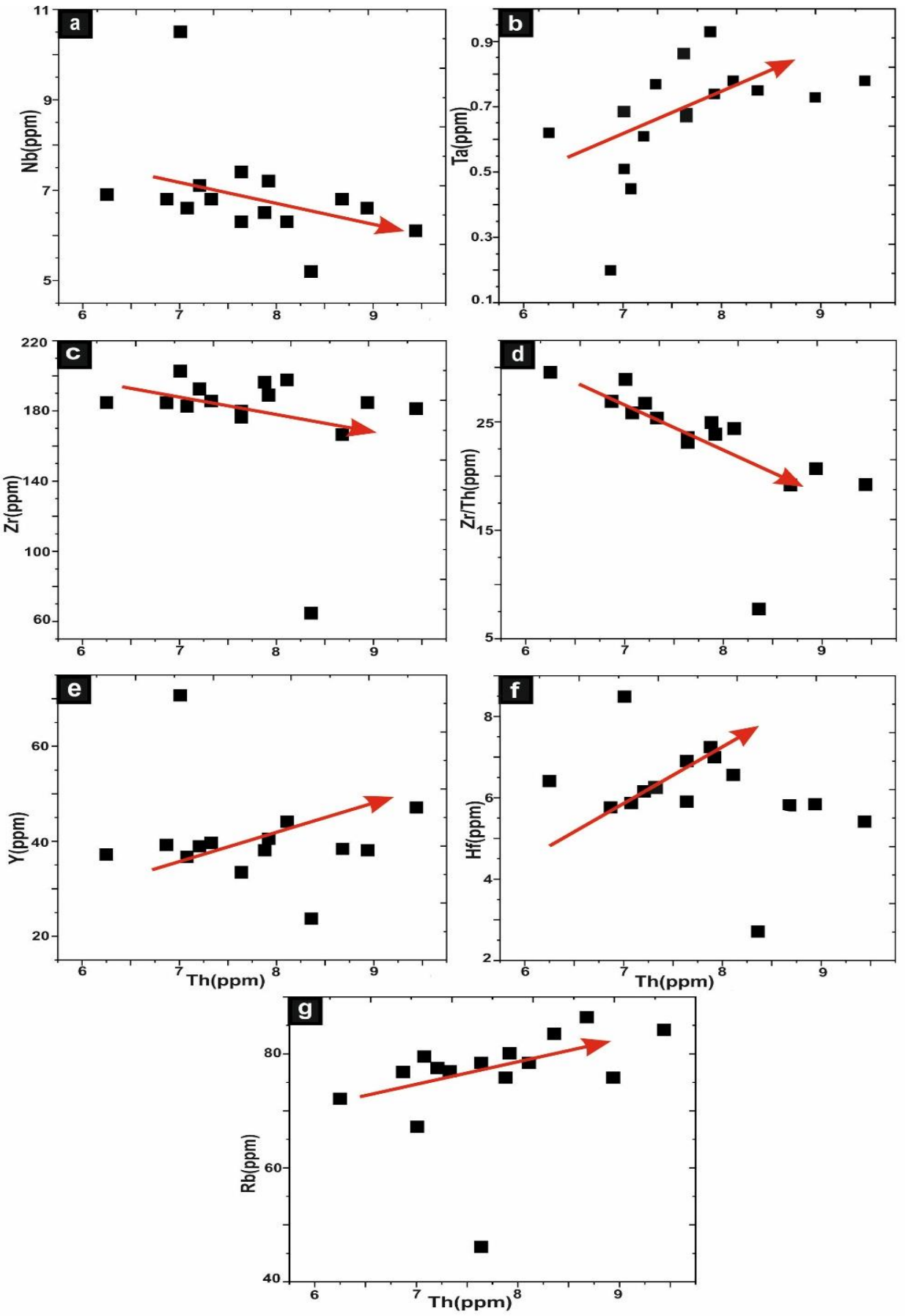

Fig. (12a-g): Variation diagrams between Th (ppm) vs. some trace elements (ppm) of monzo-syenogranites of Wadi El-Nabi'.

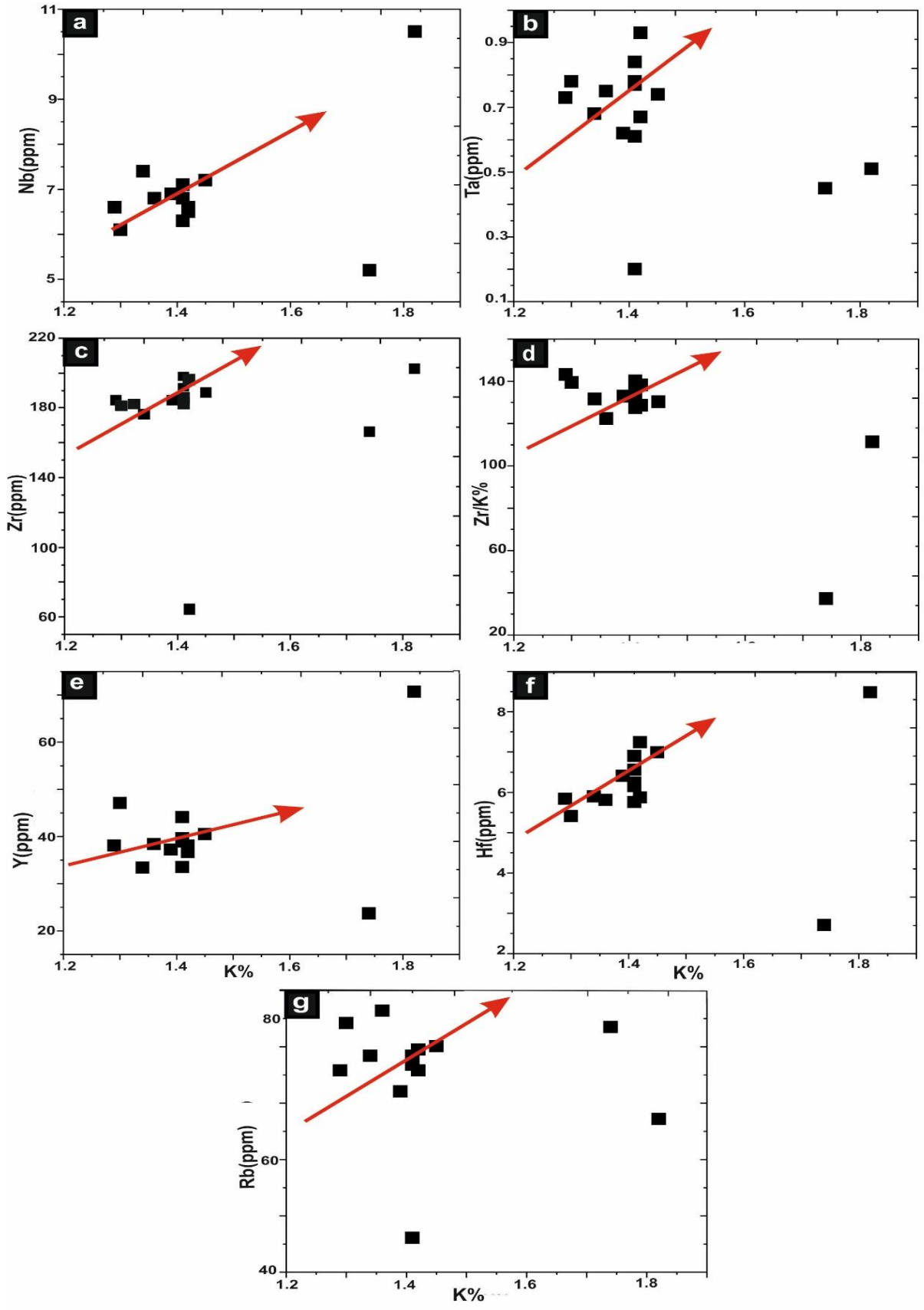

Fig. (13a-g): Variation diagrams between K% vs. some trace elements (ppm) for monzo-syenogranites of Wadi El-Nabi'.

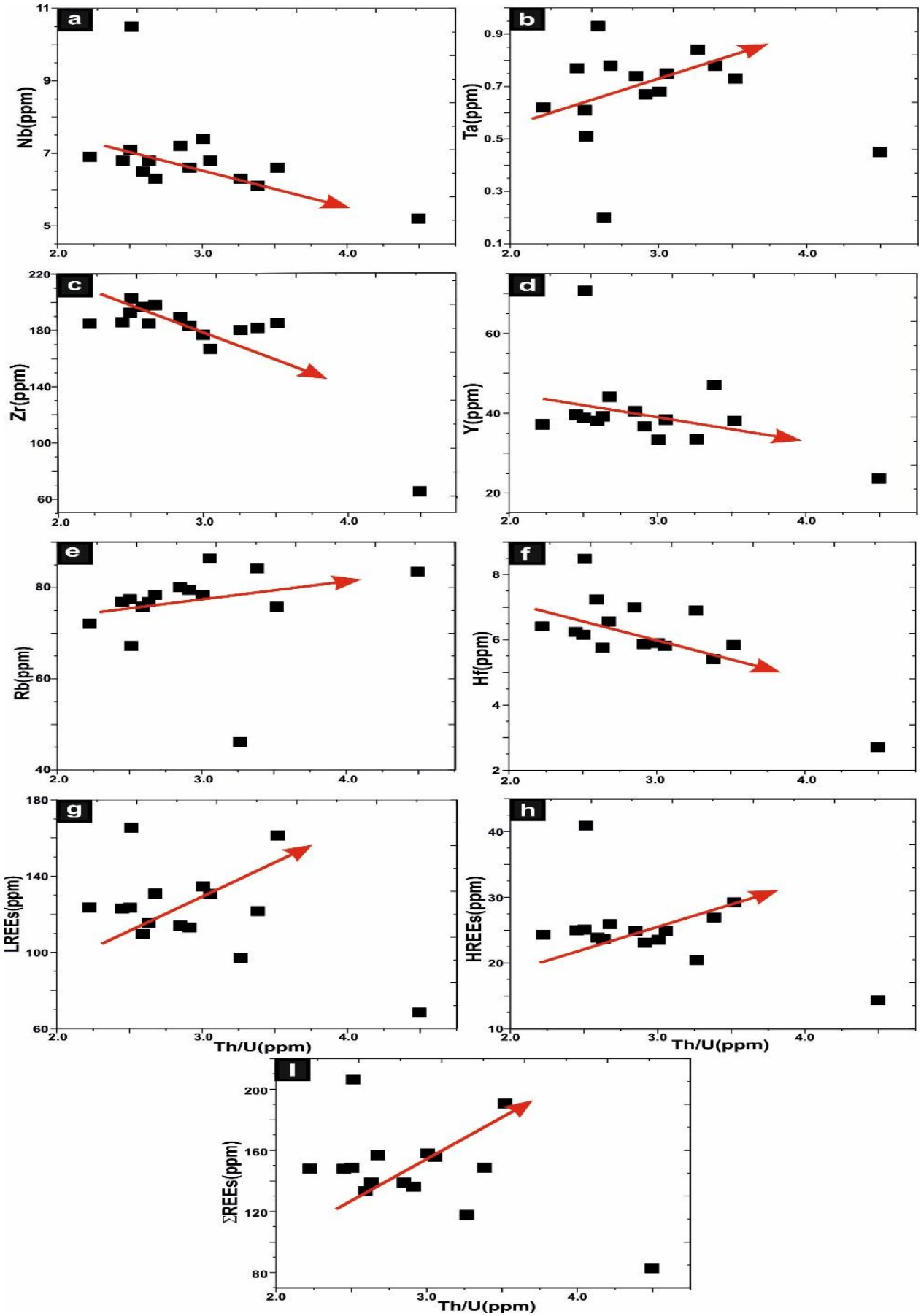

Fig. (14a-i): Variation diagrams between Th/U vs. some trace elements and rare earth elements (ppm) (REEs) of monzo-syenogranites of Wadi El-Nabi'.

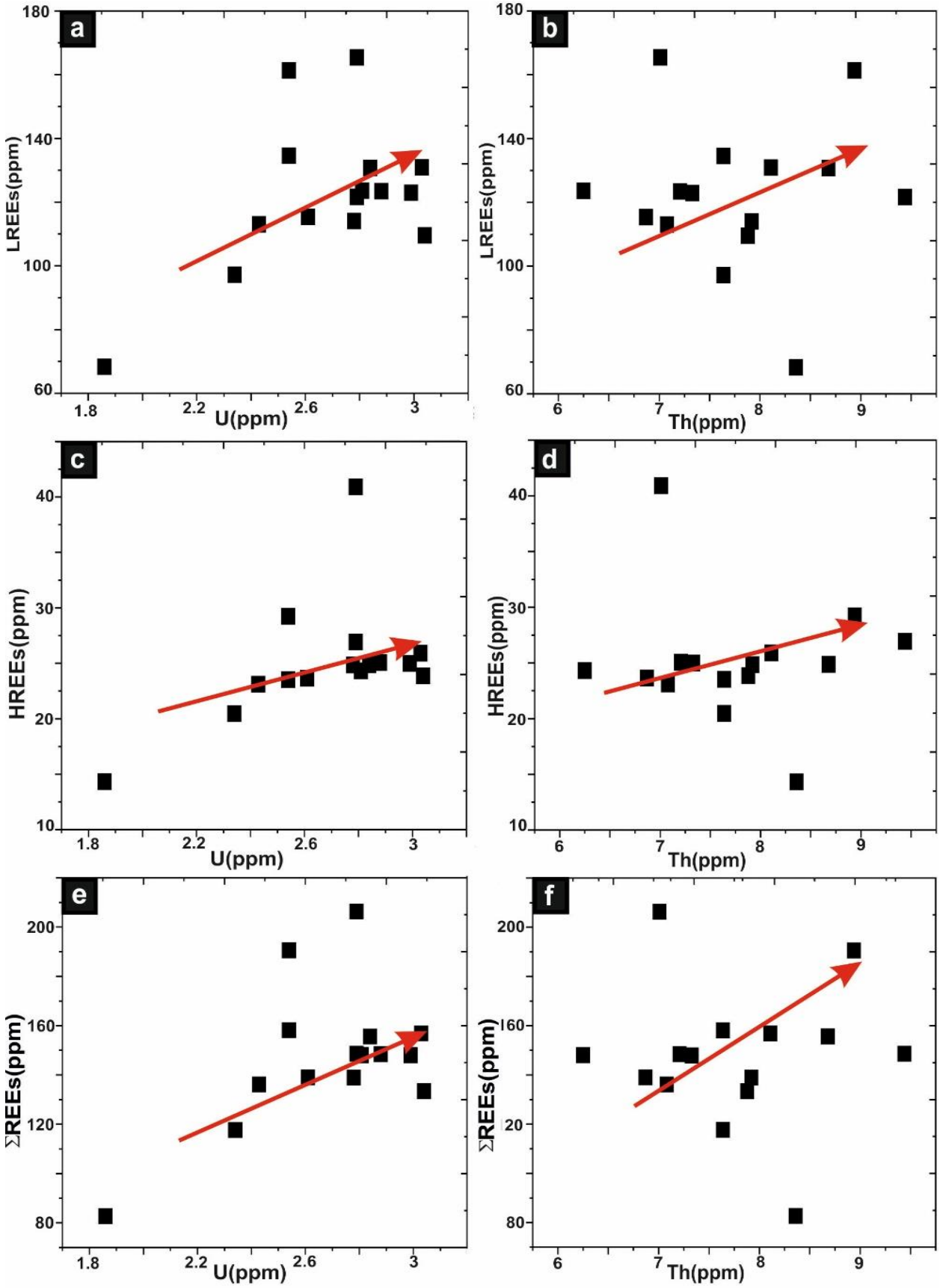

Fig. (15 a-f): Variation diagrams between U, Th (ppm) vs. rare earth elements (ppm) for monzo-syenogranites of Wadi El-Nabi'.

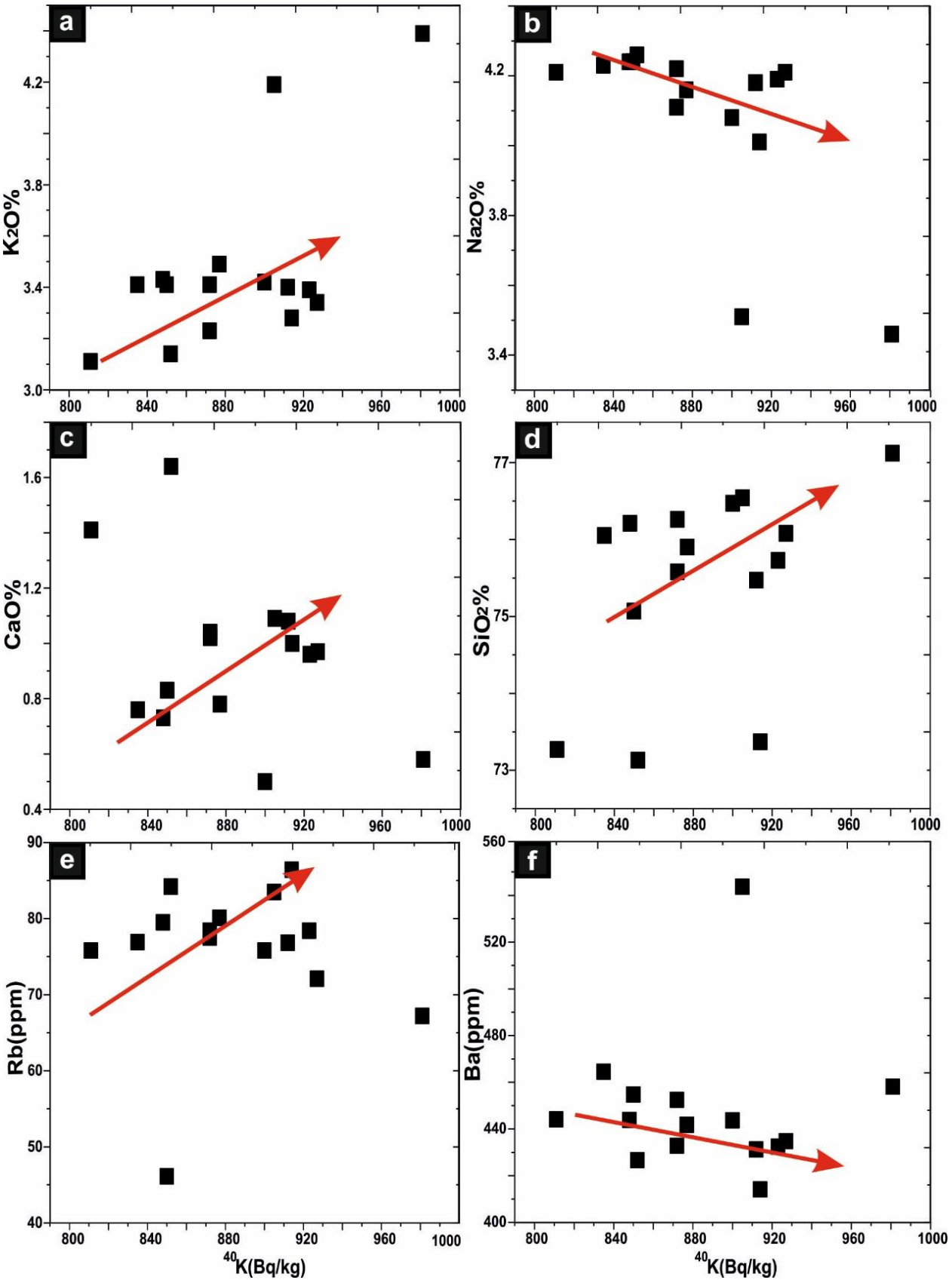

Fig. (16a-f): Variation diagrams between K^{40} (Bq/Kg) vs. major oxides (wt.%) and some trace elements (ppm) for monzo-syenogranites of Wadi El-Nabi'.

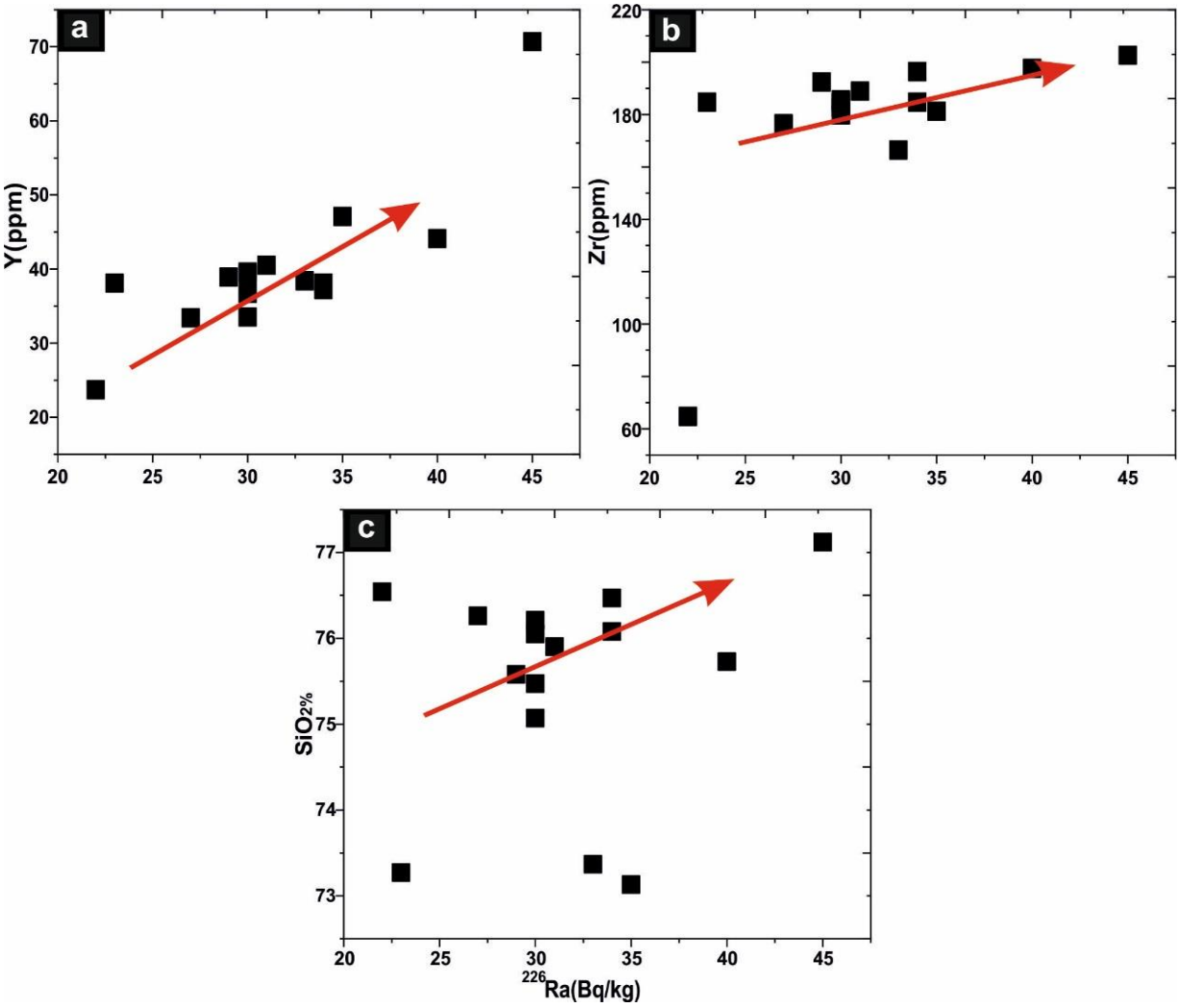

Fig. (17a-c): Variation diagrams between ^{226}Ra (Bq/Kg) and major oxides (wt.%) and trace elements (ppm) for monzo-syenogranites of Wadi El-Nabi'.

5.3. Equilibrium and disequilibrium state (P and D-factor)

5.3.1. ^{238}U/^{226}Ra equilibrium (P-factor)

To determine the concentrations of ^{238}U decay chain members and the correlation [e.g. 27 to 32]. of secular radioactive equilibrium, the equilibrium P factor after [32] and expressed as (eU/eRa). It was calculated for all studied granitic rocks giving rise to ratio > 1, which is equal to 3.52 (Table 5), reflecting a state of disequilibrium, while the unity of the P-factor indicates the state of equilibrium. The mobilization of the U radionuclides (^{238}U and ^{226}Ra) which are significantly more mobile than ^{230}Th does occur due to affecting by hydrothermal solutions. The latter is geochemically immobile and cannot be removed easily [17.20]. In the present study, the average of investigated samples has ^{226}Ra/^{238}U ratios; 0.37, i.e. < 1 (Table 4). suggesting the enrichment in ^{238}U [3, 20] as well as re-mobilization in the studied rocks. This is a good agreement by [31,32].

5.3.2. D-factor (Uc / Ur)

The second method for calculating the equilibrium/disequilibrium states has been introduced by other authors [32] who name the equilibrium (D-factor) state as the ratio between the chemically determined uranium (Uc) and the radiometrically determined (Ur): When the D-factor ratio equals unity, this means equilibrium state is achieved; whereas the factor ratio is being <1, this confirms disequilibrium state. In this work, the average Uc is 2.68 ppm (Table 2), whereas the average of Ur is 8.63 ppm (Table 5), giving rise to the average ratio is about 0.31, i.e. confirming disequilibrium state [19,20.22, 32].

Table (4): Specific activity concentrations of C_{Ra}, C_U , C_{Th}, and C_K with (Bq/Kg) of the studied monzo-syenogranites from Wadi El-Nabi' area, Central Eastern Desert, Egypt.

Sample code	Rock Type	CRa-226 (Bq/kg)	CU-238 (Bq/Kg)	CTh-232 (Bq/kg)	CK-40 (Bq/kg)	Raeq	U-238/ Ra-226	Ra-226/ U-238
G5C	MG	33	88	41	906	162	2.65	0.38
G8A	MG	45	95	47	981	187	2.12	0.48
G8D	MG	32	95	28	875	140	2.93	0.34
G15B	MG	27	0	29	844	134	0	0
G16A	MG	27	29	34	872	144	1.05	0.96
G16F	MG	27	0	32	875	140	0	0
G22B	MG	30	29	32	912	146	0.97	1
G22C	MG	29	0	31	872	140	0	0
G22D	MG	29	15	38	885	151	0.52	1.91
G24A	MG	23	104	32	811	131	4.58	0.22
G24C	MG	23	77	31	858	134	3.29	0.30
G24E	MG	21	94	23	989	130	4.44	0.22
G28B	MG	31	55	36	877	150	1.74	0.58
G44B	MG	30	96	34	835	143	3.21	0.31
G51A	MG	35	85	36	852	153	2.43	0.41
G5A	SG	33	133	29	1107	160	4.06	0.25
G5B	SG	32	126	40	911	159	3.93	0.25
G8B	SG	30	114	30	936	145	3.84	0.26
G8C	SG	41	186	41	944	172	4.54	0.22
G15A	SG	34	152	31	900	148	4.49	0.22
G15C	SG	32	177	36	960	157	5.57	0.18
G16B	SG	30	106	32	850	142	3.49	0.29
G16C	SG	28	96	34	868	143	3.46	0.29
G16D	SG	22	92	28	721	117	4.09	0.24
G16E	SG	27	165	35	695	130	6.13	0.16
G21A	SG	30	114	30	848	139	3.76	0.27
G21B	SG	35	130	38	926	161	3.68	0.27
G22A	SG	40	152	38	923	166	3.77	0.26
G23A	SG	31	158	36	899	152	5.12	0.19
G24B	SG	26	167	34	823	138	6.37	0.16
G24D	SG	27	160	36	764	137	5.88	0.17
G25A	SG	31	170	38	972	160	5.52	0.18
G33A	SG	22	175	31	905	136	7.99	0.13
G44A	SG	34	152	33	927	152	4.46	0.22
G47A	SG	33	145	42	914	163	4.36	0.23
Average	-	30.4	106.6	34.19	886.7	147.5	3.57	0.37

MG=Monzogranite **SG=Syenogranite**

Table (5): Concentrations of Ra, U, Th, and K with (ppm) of the studied monzo- syenogranites from Wadi El-Nabi' area, Central Eastern Desert, Egypt.

Sample code	Rock Type	eRa (ppm)	eU (Ur) (ppm)	eTh (ppm)	K%	eU/eRa
G5C	Monzogranite	2.98	7.11	1.02	2.89	2.39
G8A	Monzogranite	4.05	7.73	1.15	3.14	1.99
G8D	Monzogranite	2.92	7.68	6.87	2.8	2.69
G15B	Monzogranite	2.48	0	7.21	2.69	0
G16A	Monzogranite	2.47	2.33	8.49	2.78	0.99
G16F	Monzogranite	2.47	0	7.87	2.79	0
G22B	Monzogranite	2.69	2.352	7.84	2.91	0.88
G22C	Monzogranite	2.6	0	7.54	2.79	0
G22D	Monzogranite	2.6	1.23	9.27	2.83	0.47
G24A	Monzogranite	2.04	8.4	7.86	2.59	4.12
G24C	Monzogranite	2.11	6.26	7.68	2.74	2.97
G24E	Monzogranite	1.91	7.643	5.7	3.16	4
G28B	Monzogranite	2.82	4.43	8.86	2.8	1.57
G44B	Monzogranite	2.69	7.77	8.36	2.67	2.89
G51A	Monzogranite	3.17	6.91	8.95	2.72	2.18
G5A	Syenogranite	2.95	10.77	7.2	3.54	3.65
G5B	Syenogranite	2.89	10.23	9.81	2.91	3.54
G8B	Syenogranite	2.67	9.23	7.45	2.99	3.46
G8C	Syenogranite	3.68	15.02	1.01	3.01	4.08
G15A	Syenogranite	3.06	12.344	7.75	2.88	4.03
G15C	Syenogranite	2.86	14.34	8.84	3.07	5.01
G16B	Syenogranite	2.74	8.59	7.98	2.72	3.14
G16C	Syenogranite	2.48	7.73	8.44	2.77	3.12
G16D	Syenogranite	2.02	7.45	6.8	2.3	3.69
G16E	Syenogranite	2.43	13.37	8.61	2.22	5.50
G21A	Syenogranite	2.73	9.23	7.47	2.71	3.38
G21B	Syenogranite	3.19	10.561	9.35	2.96	3.3
G22A	Syenogranite	3.63	12.31	9.48	2.95	3.39
G23A	Syenogranite	2.77	12.76	8.94	2.87	4.6
G24B	Syenogranite	2.36	13.52	8.4	2.63	5.73
G24D	Syenogranite	2.45	12.97	8.81	2.44	5.29
G25A	Syenogranite	2.77	13.77	9.29	3.11	4.97
G33A	Syenogranite	1.97	14.14	7.59	2.89	7.18
G44A	Syenogranite	3.08	12.32	8.08	2.96	4
G47A	Syenogranite	2.99	11.7	1.03	2.92	3.91
Average	-	2.73	8.63	7.34	2.83	3.52

6. CONCLUSIONS

To address the characteristic signature related to the specific activity (^{238}U, ^{226}Ra, ^{232}Th and ^{40}K) and their origin for the studied El-Nabi' monzo-syenogranites, the remarkable conclusions are as follows:

1. The reconnaissance, ground survey spectrometry field points sample measurements (RS-230) detected radioactive concentrations for massive and sheared monzo-syenogranites (Table 1), in which the values of radionuclides measured by (RS-230 BOG) detector were more twice than those recorded on the chemical analysis method (Table 2). This result is consistent with published works by [20,22].

2. The results obtained from ICP-MS measurements of U/ Th and Th/U ranged from 0.22 to 0.45 ppm with an average of 0.35 ppm and from 2.22 to 4.49 ppm with an average 2.94 ppm respectively, (Table 2). The mean value of Th/U is 2.94 ppm, is lower than the world average ratio 3.5 ppm whereas the mean value of U/ Th is 0.35, which is almost equal to the global ratios 0.3 [25,26,27].

3.The obtained chemical data using ICP-MS (Tables 2 and 3) of the studied radioactive elements and other elements in the studied monzo-syenogranites confirm the same conclusions relevant to radiometric field measurements. In addition, the chemical interpretations given for many variation diagrams among U, Th, and K as well as selected major, trace and rare earth elements indicate that the magmatic process (in major) followed by the post- magmatic process (hydrothermal phase, in minor) do occur, and the later process caused redistribution and remobilization of U giving rise to enrichments [e.g., 33-34].

4. The correlation between geochemical, and radiometric data; both field using RS-230 and HPGe detector point out that the high natural radioactivity levels of the studied monzo-syenogranites appear to be closely associated with high almost trace elements and REEs contents, SiO_2 %, alkalis % which indicate proper magmatic phase followed by post-magmatic ones.

5. The P and D factors calculated of the studied radioactive elements for the monzo-syenogranites indicate the disequilibrium state, confirming recent U- enrichment.

6. the Geochemical and Spectrometric Characteristics of Natural Radioactivity Levels (^{238}U, ^{232}Th, ^{40}K) of Monzo-Syenogranites from Wadi El-Nabi' Area, Egyptian Nubian Shield could be used to update the Egyptian radiological map.

7. The given data were collected, tabulated, and analyzed using SPSS version 26. The mean and standard deviation were used to describe the variables. In addition, the correlation was calculated to measure the relation between variables. scatter plots were used to show the data behavior with the best fit line.

Acknowledgments

The authors thank the peer reviewers for their constructive comments that improved the present paper.

REFERENCES

[1] Rogers, J.J.W., and Adams, J.A.S., 1969. Uranium , and Thorium, In: Wedepohl, K.H., Ed., H, andbook of Geochemistry, Vol. 113, Springer, Berlin, 92-B-1 to 92-0-8 , and 90-Bb-1 to 90-00-5.

[2] Finch, R., , and Murakami, T., 1999. 3. Systematics , and Paragenesis of Uranium Minerals. Uranium, 91-1 80.

[3] Erkül, S. T., Ozmen, S. F., Erkül, F. , and Boztosun, I., 2016. Comparison between natural radioactivity levels , and geochemistry of some granitoids in western Turkey, Turkish J Earth Sci., 25, pp. 242-255.7.

[4] Heikal, M. Th. S., Mahmoud, K. R., El-Sobky, T., , and Top, G., 2016. Toward Assessment the High Gamma Dose Levels , and Relevant Human Health Impacts from Precambrian Granites, Na'wah Area, Yemen Republic. Inter. J. Env. , and Water, 5/3, pp. 1-12.

[5] 5Heikal, M. T. S., , and Top, G., 2018. Assessment of radioactivity levels , and potential radiation health hazards of Madsus granites , and associated dikes nearby , and around

[6] Ahmed NK (2005). Measurement of natural radioactivity in building materials in Qena city Upper Egypt. J Environ Radioact 83: 91- 99.

[7] Alharbi WR, Al Zahrani JH, Abbady AGE (2011). Assessment of radiation hazard indices from granite rocks of the Southeastern Arabian Shield, Kingdom of Saudi Arabia. Aust J Basic Appl Sci 5: 672-682.

[8] Tzortzis M, Haralabos T, Christofides S, Christodoulides G (2003). Gamma radiation measurements , and dose rates in commercially used natural tiling rocks (granites). J Environ Radioact 70: 223-235.

[9] Amin, M.S., 1955. Geology , and mineral deposits of umm Rus sheet. Geol. Surv. Egypt.

[10] Helba, H.A., 1994. Geochemical prospecting for rare metals in Nuweibi area, Central Eastern Desert, Egypt, Ph. D. Thesis, Alex. Univ., 145p.

[11] Abu El-Ela, F.F., 1997. Geochemistry of an isl, and-arc plutonic suite: Wadi Dabr intrusive complex, Eastern Desert, Egypt. J. African Earth Sciences, vol 24/4, 473-496.

[12] Grasty, R.L., Holman P. B., , and Blanchard Y. B., 1991. Transportable Calibration Pades for Ground , and Airborne Gamma-Ray Spectrometers. Otttawa. Geological Survey of C, anda, Paper 90-23,24 P.

[13] Killeen, P. G ., and Cameron, G. W., 1977. Computation of in situ Potassium Uranium , and thorium concentration from portable gamma ray spectrometer data. In report of activities, Part A, PP. 91-92. Otttawa, ON: Geological Survey of Canada, Paper 77-IA.

[14] Mercadier, J., Cuney, M., Lach, P., Boiron, M. C., Bonhoure, J., Richard, A. Leisen, M., , and Kister, P., 2011. Origin of uranium deposits revealed by their rare earth element signature. Terra Nova. Doi: 10.1111/j.1365-3121.2011.01008.

[15] Atwood, D. A., 2012. The rare earth elements: Fundamentals , and applications, 2012 John Wiley , and Sons Ltd, USA, 606 p.

[16] Jha, A.R., 2014. Rare earth materials: Properties , and applications, CRC press, Taylor & Francis Group, USA,329 P.

[17] Pekala, M., Kramers, J. D. , and Waber, H. N., 2010. 234U/238U activity ratio disequilibrium technique for study in guranium mobility in the Opalinus Clay at Mont Terri, Switzerl, and. Applied Radiation , and Isotopes, 68, pp. 984–992.

[18] Rudnick, R. L., Gao, S., Holl, and, H. D., , and Turekian, K. K., 2003. Composition of the continental crust. The crust, 3, 1-64.

[19] El-Afandy, A. H., El-Feky, M. G., Samia Taha, El-Minyawi, S. M. H. A. , and Salem, H. A., 2016. Distribution of Radioelements , and Evaluation of Radiological Hazard effects on Streem Sediments , and Cataclastic Rocks of Wadi Abu Rusheid, South-eastern Desert, Egypt Greener Journal of Geology , and Earth Sciences, Vol.4 (3), pp. 056-069.

[20] Heikal, M Th.S., Abedel Monsef, M., El Mansi, M., Gomaa, S.R. , and Togo., 2018. Natural Radionuclides Levels , and their Geochemical Characteristics of Abu Dabbab Albite Granite Mining Area, Central Nubian Shield of Egypt. J. Env. Hazards. Vol.1.Issue 1, pp.1-14.

[21] Papadopoulos, A., Şafak Altunkayanak, S., Koroneos, A., Alp Ünal, A., and Kamaci, O., 2017. Geochemistry of uranium, and thorium and natural radioactivity levels of the western Anatolian plutons, Turkey, Miner Petrol. DOI 10.1007/s00710-017-0492-4.

[22] Abdel-Meguid A. A., Ammar, S. E., Ibrahim, T. M. M., Ali K. G., Shahin, H. A., Omar S. A., Gaafar, I. M. E., Masoud S. M., Khamis, A. A., Haridy, M. H., Kamel, A. I., Mostafa, B. M.; Abo Donia A., Abdel-Gawad, A. E. , and Aly E. M., 2003. Uranium Potential of Eastern Desert Granites, Egypt. NMA report for Model project EGY/03/014 sponsored by IAEA 270 p.

[23] Ong, Y. H., , and Shallehhuddin, B. M. J., 1988. Promising uranium in the Central Belt Area, Peninsular Malaysia, In Uranium Deposits in Asia , and the Pacific: Geology , and Exploration, Vienna, Austria, pp. 97-107, Prospects in IAEA-Tc-543/7.

[24] Boyle, R. W., 1982. Geochemical Prospecting for Thorium , and Uranium Deposits. Developments in Economic Geology 16, Elsevier, 508 P.

[25] Saleh, G.M., Emad, B.M., Abdel Kader, I.B., 2021. Geochemistry and spectrometric prospection of Younger Granites, and granitic pegmatites bearing uranium mineralization at G. Kab El Rakeb area, Central Eastern Desert, Egypt. Acta Geochim. https://org/10.1007//s1631-021-00456-4.

[26] Frimmel, H. E., Schedel, S. , and Bratz, H., 2014. Uraninite chemistry as forensic tool for provenance analysis. Applied Geochemistry 48 (2014), pp. 104–121.

[27] Clarke, S. P., Peterman, Z. E., , and Heier, K. S., 1966. Abundances of U, Th, K in "H, and book of physical constants, Clarke, S. p. (Ed.)". The Geological Society of America Memoir, 97, pp. 521-541.

[28] UNSCEAR., 1988. "United Nations Scientific Committee on the Effects of Atomic Radiation" Sources, effects , and risks of ionizing radiation. Report to the General Assembly, with annexes, United Nations, New York.

[29] Gascoyne, M. , and Schwarcz. H. P., 1986. Radionuclide migration over recent geologic time in a granitic pluton. Chem Geol., 59, pp. 75-85.

[30] Pelt, E., Chabaux, F., Innocent, C., Navarre-Sitchler, A. K., Sak P. B. , and Brantley, S. L., 2008. Uranium—thorium chronometry of weathering rinds: rock alteration rate , and Paleo-isotopic record of weathering fluids. Earth Planet SC Lett, 27, pp. 98–105.

[31] Hussein, A. H., Abdel-Moneim, A. A., Mahdy, M. A., El-Aassy, I. E. , and Dabbour, G. M., 1992. On the genesis of surficial uranium occurrences in west central Sinai, Egypt. Ore Geol. Rev. 7.

[32] Hansink, J. D., 1976. Equilibrium analysis of a s, andstone roll-front uranium deposit. In Exploration for uranium ore deposits.

[33] Manning, D. A. C., 1981. The effect of fluorine on liquidus phase relationships in the system qz-Ab-or with excess water at 1 kbar. Contrib Mineral Petrol., 76, pp. 257–262.

[34] Cuney, M., 2010. Evolution of uranium fractionation processes through time: driving the secular variation of uranium deposit types. Econ. Geol., 105, pp. 553–569.